A modeling assessment of the role of reversible scavenging in controlling oceanic dissolved Cu and Zn distributions

S. H. Little,[1,2] D. Vance,[1,2] M. Siddall,[1] and E. Gasson[1,3]

Received 4 October 2012; revised 3 June 2013; accepted 28 July 2013; published 18 August 2013.

[1] The balance of processes that control elemental distributions in the modern oceans is important in understanding both their internal recycling and the rate and nature of their eventual output to sediment. Here we seek to evaluate the likely controls on the vertical profiles of Cu and Zn. Though the concentrations of both Cu and Zn increase with depth, Cu increases in a more linear fashion than Zn, which exhibits a typical "nutrient-type" profile. Both elements are bioessential, and biological uptake and regeneration has often been cited as an important process in controlling their vertical distribution. In this study, we investigate the likely importance of another key vertical process, that of passive scavenging on sinking particles, via a simple one-dimensional model of reversible scavenging. We find that, despite the absence of lateral or vertical water advection, mixing, diffusion, or biological uptake, our reversible scavenging model is very successful in replicating dissolved Cu concentration profiles on a range of geographic scales. We provide preliminary constraints on the scavenging coefficients for Cu for a spectrum of particle types (calcium carbonate, opal, particulate organic carbon, and dust) while emphasizing the fit of the *shape* of the modeled profile to that of the tracer data. In contrast to Cu, and reaffirming the belief that Zn behaves as a true micronutrient, the scavenging model is a poor match to the shape of oceanic Zn profiles. Modeling a single vertical process simultaneously highlights the importance of lateral advection in generating high Zn concentrations in the deep Pacific.

Citation: Little, S. H., D. Vance, M. Siddall, and E. Gasson (2013), A modeling assessment of the role of reversible scavenging in controlling oceanic dissolved Cu and Zn distributions, *Global Biogeochem. Cycles*, *27*, 780–791, doi:10.1002/gbc.20073.

1. Introduction

[2] The factors that control the distribution of trace metals are of prime importance to the biogeochemistry of the oceans [*Bruland and Lohan*, 2003], including the potential control these micronutrients exert on the intermediate timescale carbon cycle [*Morel et al.*, 2003; *Morel and Price*, 2003]. The oceanic behavior and distribution of these trace metals have been studied since analytical advances in the early 1970s made possible robust determination of their concentrations (reviewed in *Bruland and Lohan*, [2003]). The likely importance of biological uptake was quickly recognized in vertical profiles of dissolved Cd, which are conspicuously similar to those of the major nutrients [*Boyle et al.*, 1976; *Bruland et al.*, 1978; *Martin et al.*, 1976]. In fact, concentrations of many trace metals increase with depth (including Zn, Cu, Ni, and Fe). This observation, given the known role of many metals as micronutrients [e.g., *Morel et al.*, 1991, 2003], is frequently explained by recourse to the process of biological uptake and regeneration [*Collier and Edmond*, 1984]. It is accepted that Fe is limiting for phytoplankton in some parts of the global ocean [*Boyd et al.*, 1996; *Martin and Fitzwater*, 1988], and there is evidence that low concentrations of Zn [*Anderson et al.*, 1978; *Brand et al.*, 1983; *Morel et al.*, 1994; *Sunda and Huntsman*, 1992] may also limit phytoplankton growth, though this hypothesis remains controversial [e.g., *Ellwood and Van den Berg*, 2000]. Moreover, the shallow recycling of Cu has been attributed to biology based on the agreement of Cu concentrations, Cu:C ratios, and Cu:PO_4 ratios in cultured and harvested North Pacific phytoplankton, and in nutricline water samples [*Sunda and Huntsman*, 1995a].

[3] The dissolved concentrations and distributions of trace metals in the oceans do not solely reflect biological activity, however. *Bruland and Lohan* [2003] review the combinations of processes of potential importance, including external sources to the ocean, internal recycling, complexation with organic ligands, and removal processes in the water column. Superimposed on these first-order vertical processes is the ocean circulation, i.e., lateral transport within water masses. The key removal process, other than

[1]School of Earth Sciences, University of Bristol, Bristol, UK.
[2]Now at Department of Earth Sciences, Institute of Geochemistry and Petrology, Zürich, Switzerland.
[3]Now at Climate System Research Center, University of Massachusetts, Amherst, Massachusetts, USA.

Corresponding author: S. H. Little, Department of Earth Sciences, Institute of Geochemistry and Petrology, NW D81.4, Clausiusstrasse 25, CH-8092 Zürich, Switzerland. (susan.little@erdw.ethz.ch)

©2013 The Authors. *Global Biogeochemical Cycles* published by Wiley on behalf of the American Geophysical Union.
This is an open access article under the terms of the Creative Commons Attribution License, which permits use, distribution and reproduction in any medium, provided the original work is properly cited.
0886-6236/13/10.1002/gbc.20073

Table 1. List of Data and Associated References Collated for Use in Modeling[a]

Basin	Cruise/Vessel	Station ID(s) (#)	Date Sampled	Cu	Zn	Reference
NE Pacific	H-77	17	Sep-77	y	y	*Bruland* [1980]
	C-I	-	Mar-78	y	y	*Bruland* [1980]
	C-II	-	Jul-78	y	y	*Bruland* [1980]
	VERTEX VII	Line T [4]	Jul/Aug-87	y	y	*Martin et al.* [1989]
	C.S.S. John Tully	Lines P and Z [9]	Feb/Sep-99	n	y	*Lohan et al.* [2002]
N Pacific	KH-00-3	Line BO [7]	Jun/Jul-00	y	y	*Ezoe et al.* [2004]
N Atlantic	JGOFS: RV Atlantis II	47°N 59°N	May/Jul-89	y	y	*Martin et al.* [1993]
	RRV Challenger 76/91	13	Mar-91	n	y	*Ellwood and Van den Berg* [2000]
	MERLIM: RV Pelagia	9	Mar-98	n	y	*Ellwood and Van den Berg* [2000]
E Atlantic	RV Meteor	4 5	Apr-90	y	n	*Yeats et al.* [1995]
S Atlantic	RV Meteor	7 9	Mar-90	y	n	*Yeats et al.* [1995]
SW Indian	Charles Darwin 15/86	2 3 4 7	Aug-86	y	y	*Morley et al.* [1993]
Southern Ocean	JGOFS ANT X/6	9xx [5]	Nov-92	y	y	*Löscher* [1999]
	IPY ANT-XXIV/3	PS104-6 PS163-1 PS113-2	Feb/Mar-08	n	y	*Zhao* [2011]
	ANT24-3 PS71	1xx [9]	Feb/Mar-10	n	y	*Croot et al.* [2011]
	ANT24-3 PS71	2xx [4]	Apr-10	n	y	*Croot et al.* [2011]

[a]See also Figure 1. VERTEX, Vertical Transport and Exchange Study; JGOFS, Joint Global Ocean Flux Study. RV, Research Vessel; IPY, International Polar Year; ANT, Antarctic; MERLIM, Marine Ecosystems Regulation: Trace Metal and Carbon Dioxide Limitations Study.

active biological uptake, is passive scavenging on sinking particles, and predicting the fate of trace elements on sorption to such particles is a topic with a considerable early literature [*Balistrieri et al.*, 1981; *Boyle et al.*, 1977; *Clegg and Whitfield*, 1990; *Craig*, 1974; *Hunter*, 1983]. More recently, it has been suggested that all metals except Cd associated with biogenic particles are adsorbed to surfaces and are not intracellular [*Yang et al.*, 2012]. *Bacon and Anderson* [1982] considered a spectrum of scavenging models, from irreversible uptake to reversible exchange, in their attempt to explain the vertical distributions of dissolved and particulate Th isotopes. They conclude that the close to linear increase in concentration of both phases with depth is consistent with continuous exchange of Th between seawater and particle surfaces, so-called "reversible scavenging." The extent to which passive scavenging and biological uptake control depth profiles of trace metals in the ocean is of fundamental importance to their marine chemistry, since it controls both their recycling within the water column and the nature and rate of the eventual output from the dissolved pool to the sediment. In this study, we investigate the extent to which reversible scavenging could explain the dissolved concentration profiles of Cu and Zn, using a simple one-dimensional modeling approach simi-

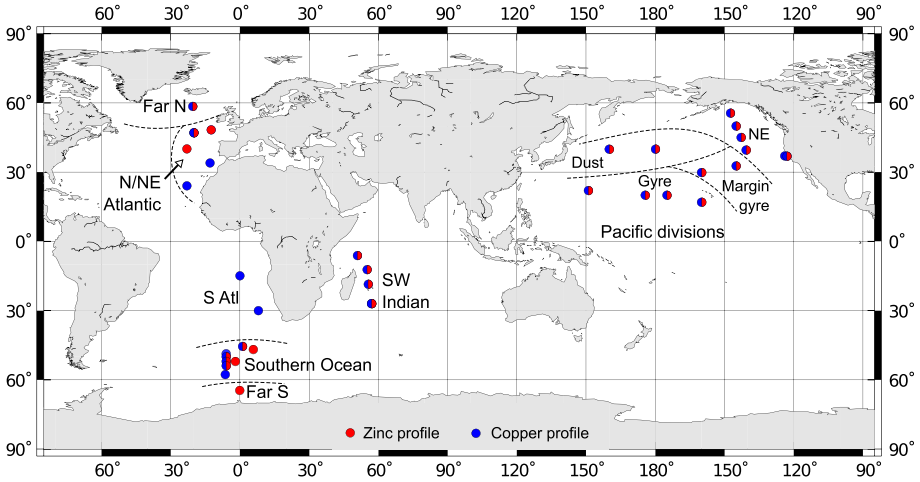

Figure 1. Map showing the location of modeled dissolved Cu (blue circles) and Zn (red circles) concentration profiles. Dashed lines and labels illustrate regional divisions chosen after selecting particle export flux values from the maps of *Sarmiento and Gruber* [2006], as summarized in Table 3. Data sources are summarized in Table 1. A large data set for Zn in the Atlantic sector of the Southern Ocean is not shown in this figure and was not modeled due to the presence of sufficient Zn data from other studies for this region [*Croot et al.*, 2011].

Table 2. Summary of Variables Used in Reversible Scavenging Model

Symbol	Units	Value	Comments
[Cu] or [Zn]	nmol kg^{-1}	-	Measured dissolved Cu/Zn concentration
q	-	-	Representation of reversible scavenging
L	-	-	Physical transport (advection, convection, and diffusion)
t	s	-	Time
z	m	-	Depth (positive downward)
z_0	m	100	Base of euphotic zone
		Dissolution Profiles	
w_s	m yr^{-1}	1000	Particle settling rate
J	-	C, 12.01 Si, 28.09	Molar mass of particle type
F	mol (or g) m^{-2} yr^{-1}	See Table 3	Particulate flux out of euphotic zone
M	g m^{-3}	JF/w_s	Particulate mass
ρ_{sw}	kg m^{-3}	1027	Density of seawater
R	-	M/ρ_{sw}	Particulate concentration (dimensionless)
$z_p o$	m	2000	Penetration depth, $CaCO_3$
$z_p o$	m	10,000	Penetration depth, Opal
		Scavenging Model	
C	nmol kg^{-1}	$\approx C_d$ at z_0	Total tracer concentration
C_p	nmol kg^{-1}	$[S/(S+1)]\times C$	Particle-associated tracer concentration
C_d	nmol kg^{-1}	-	Dissolved tracer concentration
K	-	K_{CaCO3} (1-10^8) K_{opal} (1-10^8) K_{POC} (1-10^7) K_{dust} (1-10^7)	Particle scavenging coefficients, (random starting values)
S	-	-	The product of K and R

lar to that of *Bacon and Anderson* [1982]. This approach has been used with success to replicate vertical distributions of Pa/Th [*Marchal et al.*, 2000; *Siddall et al.*, 2005] and Nd isotopes [*Siddall et al.*, 2008], within global ocean models. *A priori*, it is expected that biological cycling dominates [Zn] distributions, though a role for scavenging has been suggested [*Balistrieri et al.*, 1981; *Hunter*, 1983; *Yang et al.*, 2012]. Cu distributions have previously been more strongly linked to scavenging [*Boyle et al.*, 1977; *Bruland and Lohan*, 2003].

2. Background, Philosophy, and Approach

2.1. Characteristics of and Likely Controls on Depth Profiles of Cu and Zn

[4] Dissolved Zn has a typical "nutrient-type" distribution in seawater. Deep-ocean concentrations are up to 1400 times those at the surface, and there is a strong interbasin fractionation between the deep North Atlantic and North Pacific—concentrations increase by a factor of 5–7 between the two basins (Figure 2b) [*Bruland*, 1980; *Bruland and Franks*, 1983; *Bruland et al.*, 1994; *Lohan et al.*, 2002; *Martin et al.*, 1989, 1993; *Morley et al.*, 1993]. Zinc concentrations are correlated with silicic acid, both being remineralized at greater depth than the labile nutrients (e.g., N, P). This relationship is not a result of Zn uptake into the diatom opal itself, however. Culturing studies have shown that the Zn/Si ratio of diatom opal is much lower than in the deep North Pacific water column and that 97–99% of the Zn incorporated into diatoms resides in organic material [*Ellwood and Hunter*, 2000]. A possible resolution of this apparent puzzle is the "sheltering" of an organic C-associated Zn pool and the release of this Zn on dissolution of the opal [*Lohan et al.*, 2002]. As well as being a micronutrient, Zn is a doubly charged cation and is therefore expected to be particle reactive. Hence, though biological cycling is clearly implicated in controlling Zn depth profiles, the extent to which scavenging contributes to the dissolved [Zn] pattern remains an open question.

[5] Copper is also a micronutrient, though the free Cu^{2+} ion is toxic at very low concentrations (greater than 10^{-11} M) [*Brand et al.*, 1986; *Moffett et al.*, 1997; *Sunda and Guillard*, 1976]. Copper has been termed the "Goldilocks" metal [*Bruland and Lohan*, 2003], because its free ion concentration is buffered by a class of organic ligands to levels "just right" for biological proliferation. In fact, organic complexation accounts for 95–99.8% of the dissolved phase of both Zn and Cu in the oceans [*Bruland*, 1989; *Coale and Bruland*, 1988; *Donat and Bruland*, 1990; *Ellwood and Van den Berg*, 2000; *Moffett and Dupont*, 2007]. Dissolved Cu increases linearly with depth and by a factor of 2–3 between the deep Atlantic and Pacific basins (Figure 2a) [*Boyle et al.*, 1977; *Bruland*, 1980; *Ezoe et al.*, 2004; *Martin et al.*, 1989, 1993; *Yeats et al.*, 1995]. *Bruland and Lohan* [2003] describe its vertical profile as hybrid between nutrient and scavenged-type; it is both biologically active and particle reactive, the latter leading to intermediate and deep water scavenging [*Boyle et al.*, 1977; *Craig*, 1974; *Yeats and Campbell*, 1983].

2.2. Approach

[6] Our intention here is not to attempt a full quantitative description of the biogeochemical cycles of Cu and Zn in the oceans. Rather, our principal objective is to assess the likely role of one specific removal process in controlling

Table 3. Particle Export Fluxes (F) Used in Modeling, as Described in Section 3.4[a]

	Particle Export Fluxes			
Basin	$CaCO_3$ (mol C m^{-2} yr^{-1})	Opal (mol Si m^{-2} yr^{-1})	POC (mol C m^{-2} yr^{-1})	Dust (g m^{-2} yr^{-1})
Pacific:				
Dust	0.25	0.85	4	40
NE Pacific	0.15	0.4	2.3	5
Gyre margin	**0.05**	**0.1**	**0.5**	**10**
Gyre	0.01	0.05	0.3	10
SW Indian	**0.04**	**0.05**	**0.4**	**1**
Atlantic:				
N/NE Atlantic	**0.07**	**0.3**	**3.8**	**5**
Far N Atlantic	0.13	0.35	6	2
SE Atlantic	0.15	0.05	1.85	5
Southern Ocean	**0.16**	**0.25**	**2**	**1**
Far S Ocean	0.04	1.5	1.8	1

[a]Regional fluxes used in the "global" model are highlighted in **bold** typeface.

their vertical cycling, that of reversible scavenging. The simple one-dimensional approach we employ is well suited to this objective while highlighting the importance of processes not included, such as the other dominant removal process, biological uptake and regeneration, and vertical and lateral advection of trace metals within water masses.

[7] One process that we do not explicitly attempt to understand is the key role that complexation to organic ligands plays in the marine biogeochemistry of Cu and Zn. Though a large proportion of the dissolved inventory of both these metals is complexed in this way [*Bruland*, 1989; *Coale and Bruland*, 1988, 1990; *Ellwood and Van den Berg*, 2000; *Moffett and Dupont*, 2007], it is the nonorganically complexed portion that is generally thought to be involved in the processes controlling their removal from the surface ocean [*Sunda and Guillard*, 1976; *Sunda and Huntsman*, 1995b]. Further, the number and spatial distribution of Cu and Zn speciation studies for vertical profiles in the open ocean is limited, and their conclusions differ, for example, on the importance of Cu-binding ligands outside of the euphotic zone [cf. *Coale and Bruland*, 1988; *Moffett and Dupont*, 2007]. Those studies published to date have predominantly been carried out on samples from the North Pacific [*Coale and Bruland*, 1988; *Bruland*, 1989; *Coale and Bruland*, 1990; *Moffett and Dupont*, 2007; *Buck et al.*, 2012], with a small data set for the North Atlantic [*Moffett et al.*, 1990; *Campos and Van den Berg*, 1994; *Ellwood and Van den Berg*, 2000]. In this study, therefore, we view the organically bound portion of both metals as a reservoir that resupplies the pools that are actively involved in the passive scavenging process that we model. We will return to the impact of this simplifying assumption in section 6.

2.2.1. Tracer Conservation and the Process of Reversible Scavenging

[8] Our starting point for modeling dissolved Cu and Zn is the tracer conservation equation, which describes the relationship between the rate of change of the tracer concentration with the processes that affect this concentration. Processes might include those outlined by *Bruland and Lohan* [2003] and discussed in section 1, i.e., external sources to the ocean, internal recycling, complexation with organic ligands, and removal processes in the water column, along with transport by advection and mixing (the ocean circulation). The tracer conservation equation for a tracer with concentration C can be written simply as:

$$\frac{\partial C}{\partial t} = L(C) + q(C) \tag{1}$$

where $L(C)$ represents the physical circulation of the ocean (i.e., advection within water masses) and $q(C)$ represents the internal (vertical) cycling within the water column.

[9] As stated in section 2.2, we do not attempt a complete description of tracer conservation. Instead, we investigate the extent to which the concentration profiles of Zn and Cu can be explained by a specific internal (vertical) process, reversible scavenging, and parameterize $q(C)$ accordingly. Reversible scavenging is the passive uptake of tracer on sinking particles, which are formed in/input to the upper ocean and may dissolve with depth, thereby releasing adsorbed metal to the dissolved phase (described in section 3.4). The particle-associated tracer is assumed to be in equilibrium with the dissolved phase, with continuous exchange between the two pools [e.g., *Bacon and Anderson*, 1982]. As discussed, previous applications of a reversible scavenging model [*Bacon and Anderson*, 1982; *Marchal et al.*, 2000; *Nozaki et al.*, 1981; *Siddall et al.*, 2005, 2008] have been successful for elements whose concentrations generally increase with depth, the case for both Cu and Zn.

3. Methods

3.1. Data Sources

[10] Dissolved Cu and Zn data sources used in modeling, and considered here to be particularly robust against trace metal contamination, are listed in Table 1. Zn is especially sensitive to contamination, due to its ubiquity in man-made goods. Of all data compiled, most met the criteria we imposed for noncontamination. Excluded data have one or both of the following features:

[11] 1. Extreme enrichments of Zn in surface waters, uncorrelated with dust flux, and thought likely to result from ship-borne contamination.

[12] 2. "Spiky" concentration profiles, defined as rapid deviations from depth to depth, which are not explained by typical oceanic processes (such as mixing of contrasting water masses).

[13] Vertical profiles were modeled on a variety of geographical scales (see also section 3.5). First, individually, one-by-one. Second, grouped by region, with a region defined as an area within which particle export fluxes from the euphotic zone are assumed relatively invariant. Third, several regions were modeled simultaneously. The geographic locations of the profiles used in modeling are illustrated in Figure 1, which also illustrates, schematically, regional divisions. The Pacific, for example, is divided into four, each region labeled after a predominant characteristic. The region labeled "Dust," for example, is strongly influenced by the Gobi dust plume. The particle fluxes used in modeling are described in more detail in section 3.4.

3.2. The Input Flux

[14] Both Cu and Zn only have stable isotopes derived exclusively from sources external to the oceans at the surface (including riverine and aeolian sources), neglecting lateral and vertical transport (cf. Pa/Th isotopes) [*Siddall et al.*, 2005]. This study does not consider any potential hydrothermal input, because chalcophile elements (including Cu and Zn) are believed to be quantitatively removed close to the vent source [*Cave et al.*, 2002; *German et al.*, 1991, 2002; *Trocine and Trefry*, 1988]. Given inputs only at the surface, we make the simplifying assumption that, in the open ocean, this input flux is recorded in the average dissolved concentration at the base of the euphotic zone, which we define between 50 and 150 m water depth. For conservation, this input flux must be balanced by downward scavenging.

3.3. The Reversible Scavenging Model

[15] Variables used in the reversible scavenging model are listed in Table 2, and follow those in *Siddall et al.* [2008]. Reversible scavenging assumes that the tracer is at equilibrium with falling particles and that reversible exchange occurs between seawater and particle surfaces. This relationship can be described by an equilibrium scavenging coefficient, K, which is the ratio of the dissolved (C_d) and particulate-associated (C_p) concentrations:

$$K = \frac{C_p}{C_d R} \tag{2}$$

where R is the concentration of particulate matter. The value of R is dimensionless, being defined as the ratio of the mass of particles per cubic meter to the density of seawater. The tracer (Cu or Zn) concentrations C_d and C_p have units of nmol per kilogram of seawater, and K is therefore a distribution coefficient of tracer between the dissolved and particulate phase. Note that the total concentration C is equal to the sum of the particulate-associated and dissolved concentrations (i.e., $C = C_p + C_d$) and that a smaller K value reflects less particle-associated tracer. For such a scavenging process, q can be parameterized as follows:

$$q(C) = -\frac{\partial(w_s C_p)}{\partial z} \qquad \text{where } C_p = \left[\frac{S}{S+1}\right] \cdot C \tag{3}$$

where w_s is the particle settling velocity and $S = \Sigma KR$. In the absence of any observational data for particulate-associated Cu and Zn concentrations, C_p is calculated at the base of the euphotic zone assuming that the total concentration $C \approx C_d$ at this depth.

[16] S can be expanded to incorporate a variety of particle types, which might be expected to have differing K values for Cu and Zn, including opal, calcium carbonate, particulate organic carbon (POC), and dust. S then becomes

$$S = K_{\mathrm{POC}} R_{\mathrm{POC}} + K_{\mathrm{CaCO_3}} R_{\mathrm{CaCO_3}} + K_{\mathrm{opal}} R_{\mathrm{opal}} + K_{\mathrm{dust}} R_{\mathrm{dust}} \tag{4}$$

after *Siddall et al.* [2005, 2008].

[17] Mass balance with the input flux is achieved through the process of downward scavenging, and depends on the particle-associated concentration C_p (equation (3)). Assuming steady state, and a uniform settling velocity, the implication is that C_p must be constant with depth. Rearranging equation (2):

$$C_d = \frac{C_p}{KR} \tag{5}$$

K also remains constant with depth, while the particulate concentration R decreases (as the particles dissolve). As a result, the dissolved concentration, C_d, must increase, reflecting the specific particle dissolution profiles imposed.

3.4. Particle Dissolution Profiles

[18] Four particle types are included in the model: calcium carbonate, opal, particulate organic carbon (POC), and dust. Export fluxes F (i.e., fluxes sinking out of the euphotic zone) for each particle type vary geographically according to biological productivity and ecosystem dynamics, and for dust, to the proximity of atmospheric dust plumes. Different ocean regions (see Figure 1) are thus subject to differing export fluxes, as summarized in Table 3. Dust fluxes (in g m^{-2} yr^{-1}) were taken from the Global Ozone Chemistry Aerosol Radiation Transport (GOCART) model simulations [*Ginoux et al.*, 2001]. Export fluxes for the biogenic particle types (in mol C or Si m^{-2} yr^{-1}) were selected from maps plotted by *Sarmiento and Gruber* [2006]. *Sarmiento and Gruber* [2006] calculate POC export from the empirical algorithm of particle export ratio to primary production reported in *Dunne et al.* [2005]. Their opal and carbonate fluxes are then calculated using estimates of opal and carbonate to POC export ratios, also from *Dunne et al.* [2005].

[19] On sinking out of the euphotic zone, the biogenic particles dissolve, or are regenerated via grazing by zooplankton. This dissolution for POC and $CaCO_3$ is parameterized as in the previous studies of *Henderson et al.* [1999], *Marchal et al.* [2000], and *Siddall et al.* [2005]. $CaCO_3$ is described by an exponential penetration profile with penetration depth ($z_p c$) of 2,000 m [*Henderson et al.*, 1999], and POC by a power law (exponent b) [*Berelson*, 2001; *Marchal et al.*, 2000; *Martin et al.*, 1987], both with respect to depth (z, positive downward). *Sarmiento and Gruber* [2006] derive an empirical dissolution profile for opal based on sediment trap data, and related by a linear factor to the POC power law. An earlier parameterization of opal dissolution utilizes an exponential penetration profile like that described for $CaCO_3$, with penetration depth for opal ($z_p o$) of 10,000 m [*Henderson et al.*, 1999]. Results reported in this study are based on the empirical opal dissolution profile of *Sarmiento and Gruber* [2006], but these results are compared to those obtained using the exponential profile in section 5 (sensitivity testing).

[20] The biogenic particulate mass, M (in mol C or Si m^{-3}), is related to the particulate flux F, the molar mass J, and the settling rate w_s (in m^{-3} yr^{-1}), such that $M = JF/w_s$ [*Siddall et al.*, 2005]. Dissolution profiles with respect to depth for the three biogenic particle types are therefore as follows:

$$M_{CaCO_3}(z) = M_{CaCO_3}(z_0) \exp\left(\frac{z_0 - z}{z_p c}\right) \quad (6)$$

$$M_{POC}(z) = M_{POC}(z_0) \cdot \left(\frac{z}{z_0}\right)^{-b} \quad (7)$$

$$M_{opal}(z) = M_{opal}(z_0) \cdot p_e \cdot z_0^b \cdot z^{-0.448} \quad (8)$$

$$\text{Or } M_{opal}(z) = M_{opal}(z_0) \exp\left(\frac{z_0 - z}{z_p o}\right) \quad (9)$$

where z_0 is the depth of the euphotic zone, taken as 100 m, and p_e is the particle export ratio. The exponent for POC dissolution, b, is 0.858 [*Martin et al.*, 1987].

[21] Dust is assumed not to dissolve significantly with depth. Our main motivation in including a dust flux is to simulate the sorptive capacity of Fe and Mn oxides that coat the surface of dust particles. Though these oxides are a minor component of the total particulate flux, they have a strong affinity for doubly charged cations like Cu and Zn [*Catts and Langmuir*, 1986; *Tessier et al.*, 1985, 1996].

3.5. Model Optimization

[22] Modeling of dissolved Cu and Zn concentrations is carried out for all data points below the euphotic zone ($z > z_0$). To optimize the reversible scavenging model for its effect on Cu and Zn concentration profiles, we vary the equilibrium scavenging coefficients (K values) for the four particle types. We then consider the resulting [Zn] and [Cu] distributions via a cost function (σ), which is the root-mean squared deviation of the model from the data. To do this, we use the function "fmincon" in the MATLAB optimization toolbox. This function attempts to find a constrained minimum of a scalar function of several variables starting at an initial estimate, within a region specified by linear constraints and bounds. In our case, it selects optimal values for K_{POC}, K_{opal}, K_{CaCO3}, and K_{dust}:

$$\sigma = \sqrt{\Sigma(\text{data} - \text{Model})^2} \quad (10)$$

As stated in section 3.1, modeling (i.e., optimization of K values) was carried out on a variety of scales, including for individual profiles, for the four regions of the North Pacific, and for (close to) the entire global data set. Where simultaneous modeling of more than one profile from the same region/multiple regions was attempted, individual profiles were aggregated and modeled as a single data set. For the "global" model, the N/NE Atlantic and the Far N Atlantic profiles, and the NE Pacific and Pacific gyre margin profiles were combined and modeled simultaneously with those of the SW Indian Ocean and those of the Southern Ocean. Where two regions were combined (i.e., in the North Atlantic and North Pacific), the lower of the two export flux estimates for the two regions was used (see Table 3). This is justified in part by the observation for Th that, where particle concentrations are high, K_d values are systematically lower than in areas with lower particulate concentrations [*Guo et al.*, 1995; *Honeyman et al.*, 1988]. Combining regions allows the inclusion of a larger data set in the "global" model, while, in order to avoid a bias toward one particular region, the sum of the aggregated data points for each region was targeted at $n \approx 100$. This was possible for all cases except for Cu in the Southern Ocean, where $n = 76$, and for Zn in the Atlantic Ocean, where $n = 42$.

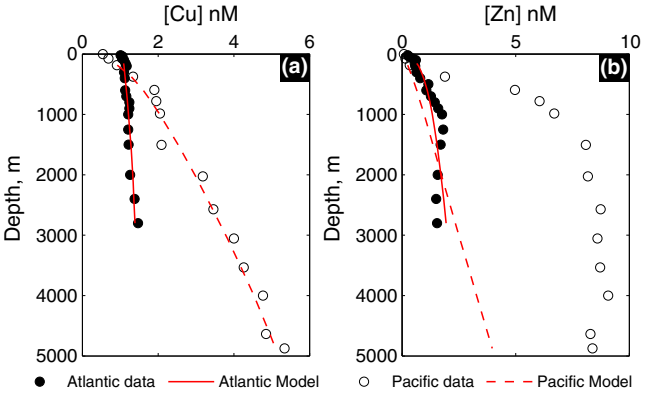

Figure 2. Typical dissolved (a) Cu and (b) Zn concentration profiles (filled circles, Atlantic; open circles, Pacific) from the Atlantic and Pacific basins, with optimized fits (solid red line, Atlantic; dashed red line, Pacific) achieved using the reversible scavenging model. Measured [Zn] shows strong depletions in surface waters and enrichment at depth and between the two basins, and is not well matched by the scavenging model. Measured Cu concentrations increase linearly and are well reproduced by the scavenging model. Data for the Atlantic are from 59°N [*Martin et al.*, 1993], and for the NE Pacific from site H77 [*Bruland*, 1980].

[23] Optimized K values show sensitivity to the initial values. To counter this, we randomize selection of initial K values and apply the optimization function iteratively in order to better constrain the best fit. Section 5 includes a more in depth discussion of this, and of the sensitivity of the model to other given parameters. The observation that there may be multiple minima in K values is not surprising, however. Findings for Nd, for example, implicated zero scavenging by POC. This was attributed to the similarity of the dissolution profiles for POC and $CaCO_3$, and the potential for the erroneous attribution of scavenging by POC to $CaCO_3$ in the model [*Siddall et al.*, 2008]. Final K values reported in this study are thus tentative and require independent observational constraints. Rather, we prefer to reflect on the relative success or otherwise of the technique in replicating measured tracer concentration profiles in order to learn something about the process at first order, i.e., is it plausible that reversible scavenging can explain a significant proportion of the variability in observed dissolved concentrations of Cu and Zn?

4. Results

[24] Comparisons of the optimized reversible scavenging model results with observational data are illustrated on a local scale for both Cu and Zn in Figure 2. Two representative individual vertical profiles from the Atlantic and Pacific are modeled, the profile from the far North Atlantic of

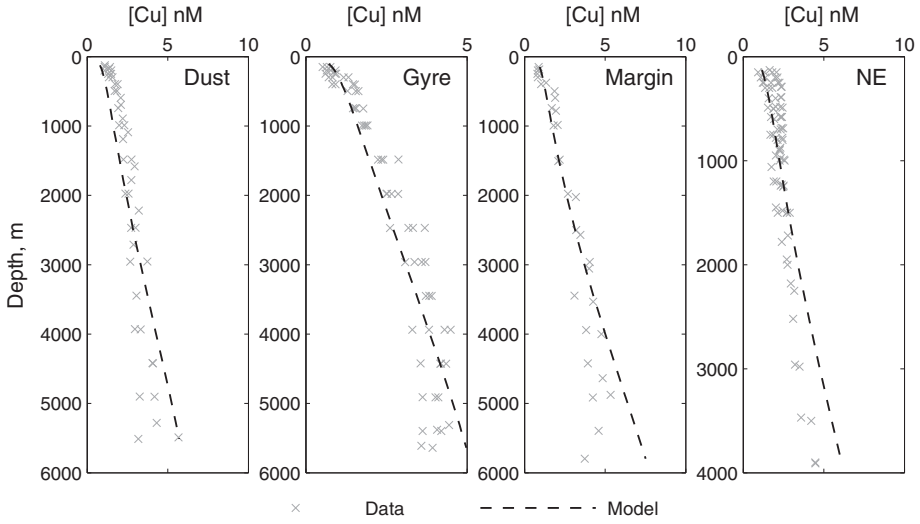

Figure 3. Results of the reversible scavenging model for simultaneous modeling of Cu in the four regions of the North Pacific, as labeled.

Martin et al. [1993], and that of site H77 in the "margin gyre" region of the Northeast Pacific [*Bruland*, 1980]. Similar optimized model results can be achieved for other individual profiles throughout the Atlantic, Pacific, and Indian Oceans. Figure 2 shows that, on the scale of an individual profile, the distribution of dissolved Cu can be matched extremely well by the reversible scavenging model. In contrast, the overall shape of the Zn profiles, with extreme depletions in surface waters, mid-depth maxima, and fairly constant Zn beneath, is not reproduced. In addition, the very high deep Pacific dissolved Zn concentrations are not matched by the model. This is due to the small Zn input, which, in the model, stems directly from very low average [Zn] in the surface ocean at site H77 (at 0.15 nmol kg^{-1}). Arbitrarily increasing the Zn input permits the model to generate deep water concentrations as high as the observed values (8–10 nM), but the modeled profile remains close to linear.

[25] Next, the model (for Cu only) was expanded to include all four regions of the North Pacific. While Cu concentration profiles are relatively similar throughout the N Pacific, particle export fluxes for the four regions are diverse (see Table 3). This variability in export fluxes introduces strong constraints on the set of K values selected by the optimization tool. The model results compared to observed dissolved Cu concentrations for the four Pacific regions are illustrated in Figure 3. It shows that, despite the regional variation in particle export fluxes, it remains possible to find a single set of K values that describe the collated Cu data for this basin relatively well. The K values selected (using the empirical dissolution profile for opal of *Sarmiento and Gruber* [2006]) are the following: $K_{CaCO3} = 7.8 \times 10^7$, $K_{opal} = 1.7 \times 10^7$, $K_{POC} = 0$, and $K_{dust} = 2.6 \times 10^4$.

[26] Finally, the results for the "global" data set are illustrated for Cu and Zn in Figure 4. Once again, observed Cu on this scale is well matched by the reversible scavenging

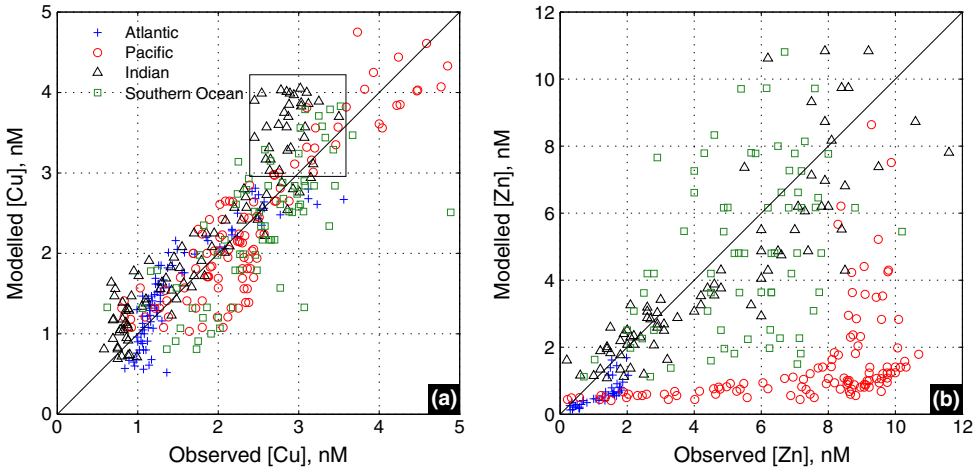

Figure 4. Fits of the reversible scavenging model to the global data sets of dissolved (a) Cu and (b) Zn. The solid line is the 1:1 relationship predicted for a perfect match of model to data. For Cu, the data and model match remarkably well, even at this global scale. Boxed Indian Ocean data are discussed in the text. For Zn, the fit is poor, especially in the Pacific.

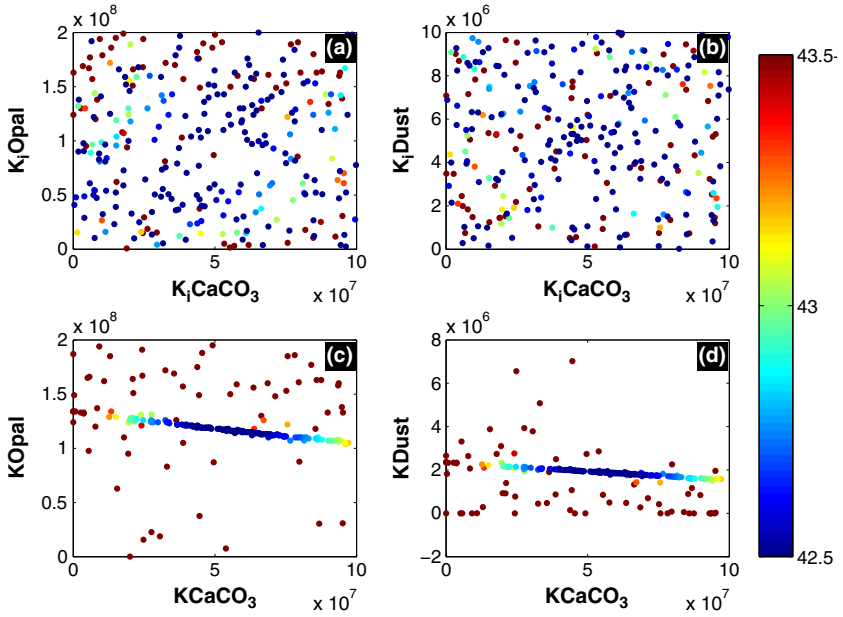

Figure 5. The effect of varying the starting values of scavenging coefficients on the optimization of these K values, as illustrated for modeling the global data set of [Cu]. (a and b) The randomly selected starting K_i values generated by the model, in K_iCaCO$_3$–$K_i$opal and K_iCaCO$_3$–$K_i$dust space. (c and d) The optimized K values output by the model using these starting values. Both pairs of plots are color coded for the final error (or cost function σ) associated with the *optimized* fit, which in this case has σ = 42.5, for K_{CaCO3} = 5.4 × 10^7, K_{opal} = 1.2 × 10^8, and K_{dust} = 1.9 × 10^6. K_{POC} is not shown, since this fit implicates no scavenging by POC.

model. This is despite the fact that both export fluxes and absolute Cu concentrations vary widely. Optimized K values for the global Cu data set, using the empirical dissolution profile for opal of *Sarmiento and Gruber* [2006], are as follows: K_{CaCO3} = 5.4 × 10^7, K_{opal} = 1.2 × 10^8, K_{POC} = 0, and K_{dust} = 1.9 × 10^6. These K values lead to a small deviation between model and observations in the southwest Indian Ocean (boxed data, Figure 4a). Observed concentrations reach a maximum at approximately 3000 m and remain constant thereafter, deviating from the linear increase that is both predicted by the model and that is typical of the observations at other locations (e.g., Figure 2a). The likely applicability of these global K values for Cu is discussed in more depth in section 5, but we note here that they should be considered preliminary. We find absolute optimized K values to be sensitive to a range of factors, including the precise data set modeled—both to the selection of concentration profiles, and to the regions included—compare optimized K values for the global data set with those of the Pacific data set. In general, however, we note that dissolved Cu can be well described by the process of reversible exchange on particle surfaces.

[27] In contrast to Cu, the reversible scavenging model is unsuccessful in matching profiles of dissolved [Zn], at either the scale of an individual profile, as discussed, or on the global scale (Figure 4b). This suggests that the shape of dissolved Zn depth profiles is dominated by another process/processes, likely those of biological uptake and regeneration, and lateral advection of dissolved Zn in deep water masses.

5. Sensitivity Testing

5.1. Varying Initial K Values

[28] An inherent problem of optimization algorithms is that they may find local minima, with the initial values frequently determining the outcome [*Kirkpatrick et al.*, 1983]. To investigate this phenomenon, we developed a version of the model that generates random initial K values within specified bounds, and used the optimization tool for each set of starting values. We then consider the cost function (σ) associated with the resultant optimized scavenging coefficients. This approach is illustrated for the global Cu data set in Figure 5, with Figures 5a and 5b showing the randomized initial K values, and Figures 5c and 5d the optimized scavenging coefficients output by the model given these starting values. Both pairs of plots are color coded by the cost function of the *optimized* result. The best fit for this set of data is σ = 42.5, with no scavenging implicated by POC (total range of σ: 42.5 to 115). For this set of data, approximately 35% of the generated starting values converge on the best fit scavenging coefficients (K_{CaCO3} = 5.4 × 10^7, K_{opal} = 1.2 × 10^8, K_{POC} = 0, K_{dust} = 1.9 × 10^6). The likelihood of convergence on the best fit of a set of starting K values appears comparatively random, though loosely related to the similarity of the initial starting values to the optimized values. It is of passing interest that the optimized scavenging coefficients in K_{CaCO3} - K_{opal} space, for example, fall on a line with a negative slope (Figure 5). Increased scavenging by CaCO$_3$ is compensated for by a reduction in scavenging by opal (recalling that a smaller K value reflects less particle-associated tracer).

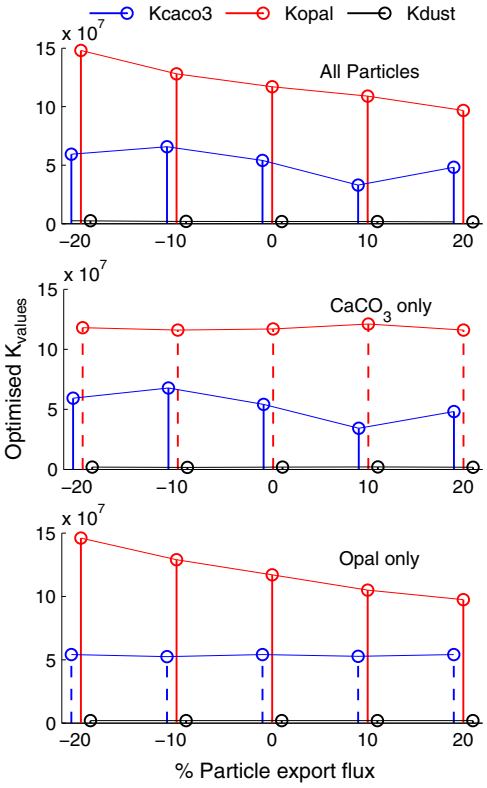

Figure 6. The impact of varying particle export fluxes between –20 and +20% of the used values on the optimized scavenging coefficients of $CaCO_3$, Opal, and Dust, for the global data set of dissolved Cu. Three scenarios are shown here: (top) varying all four particles (including POC) simultaneously, and varying (middle) $CaCO_3$ and (bottom) opal independently of the other three.

5.2. Varying Settling Rate

[29] In reality, particle dynamics in the ocean are considerably more complicated than the average settling velocity used in this study suggests. *Clegg and Whitfield* [1990] classify particulate matter into two particle groups, a course, rapidly settling group, with particle radii of >50 μm, and a fine, nonsettling, or slowly settling group, with particle radii of 1–5 μm. In terms of mass flux to the sediment, the coarse group is predominant. Settling rates of the coarse group have been estimated from analyzing sediment trap data, with rates of a few tens to 100–200 m d^{-1}. Further, it has been demonstrated that settling velocities increase with depth, from the lower to the upper end of these estimates [e.g., *Berelson*, 2001]. However, it is the fine group of particles that make up the bulk of the total particulate mass in the water column, with diameters >100 μm seen for only 1 in every 10^{10} particles [*Sarmiento and Gruber*, 2006]. Hence, on long timescales on the scale of tracer removal from the water column, particle cycling can be simplified to an average settling rate of these smaller particles. Attempts to constrain this mean settling rate have used water column measurements of particle reactive nuclides, rather than sediment trap material, because the latter captures only the rapidly settling particles. Estimates range from 0.2 to 5.3 m d^{-1} [*Krishnaswami et al.*, 1976; *Tsunogai and Minagawa*, 1978; *Mangini and Key*, 1983], with the middle of this range (3 m d^{-1}, or 1000 m yr^{-1}) used in this, and previous studies of this type [*Henderson et al.*, 1999; *Marchal et al.*, 2000; *Siddall et al.*, 2005].

[30] Export fluxes of different particles have units of mol (or g, for dust) per m^2 per year. The chosen settling rate (of 1000 m yr^{-1}) is used in calculating the steady state particulate concentration at the base of the euphotic zone ($z = z_0$). In the model, this concentration then decreases with depth according to the particle dissolution profiles imposed (except dust, which is assumed not to dissolve). The impact of decreasing the settling rate, for example, is thus to increase the steady state concentration of particulate material at any depth. This affects optimized K values, but not modeled tracer concentrations. For the global model, optimized scavenging coefficients decrease by a factor of 20 for an equivalent decrease in settling rate (1000 to 50 m yr^{-1}), but this reduction has no impact on the model fit to data, and the final cost function ($\sigma = 42.5$). Over this range, K_{CaCO3} decreases from 5.4×10^7 to 2.7×10^6, K_{opal} from 1.2×10^8 to 5.8×10^6, and K_{dust} from 1.9×10^6 to 9.5×10^4. Smaller scavenging coefficients signify an overall reduction in particle-associated tracer, therefore compensating for the reduction in settling rate (and associated increase in particulate concentrations).

5.3. Varying Particle Export Fluxes

[31] The effect of varying particle export fluxes between +20% and –20% of the used values is illustrated in Figure 6 for the global data set for dissolved Cu. We evaluate this for four scenarios: varying the fluxes of all four particle types simultaneously and varying each independently of the other three (excluding POC, for which no scavenging is implicated when using the *Sarmiento and Gruber* [2006] opal dissolution profile). The effect of reducing particle flux is similar to that observed for decreasing settling rate, that of a general reduction in optimized K values (i.e., an overall decrease in particle-associated Cu). The behavior is not linear in this case, however; and the final cost function varies by approximately ±10%. Note that changing the flux of one particle type independent of the other four primarily affects the scavenging coefficient of this particular particle (e.g., opal only, Figure 6). In conclusion, we note that the relative magnitudes of the optimized scavenging coefficients are sensitive to changing particle export fluxes, and not to changing settling rate. This sensitivity is implied by equation (4). In contrast, their absolute magnitudes are sensitive to both factors.

5.4. Scavenging by POC

[32] In the results, optimized K values for the global Cu data set are given as $K_{CaCO3} = 5.4 \times 10^7$, $K_{opal} = 1.2 \times 10^8$, $K_{POC} = 0$, and $K_{dust} = 1.9 \times 10^6$. For both this data set, and for that of the Pacific, POC is predicted to contribute no scavenging of Cu. This conclusion, if correct, is rather unexpected. Adsorption on organic materials is promoted by the negatively charged functional groups present on cell walls within most environmental pH ranges [e.g., *Fein et al.*, 1997; *Daughney et al.*, 2002]. We suggest that the attribution of zero scavenging of Cu to POC may be related instead to the similarity of the opal and POC dissolution profiles. One way to test this hypothesis is to compare the optimized K

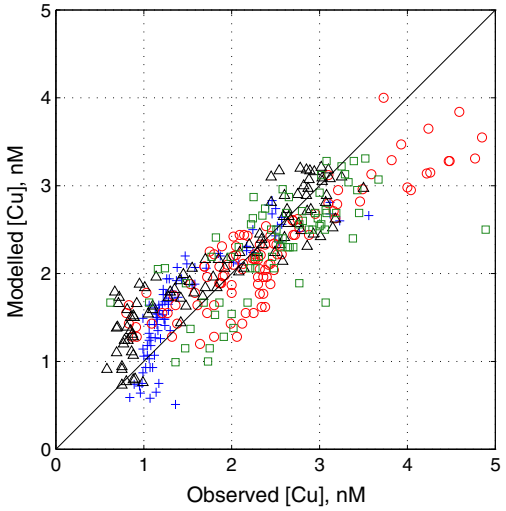

Figure 7. Fit of the reversible scavenging model to the global data set of Cu using the alternative parameterization of opal dissolution, an exponential dissolution profile with penetration depth 10,000 m (after *Henderson et al.*, 1999; *Marchal et al.*, 2000). Note similar quality of fit to that illustrated in Figure 4a.

values for the same data sets, but instead using an alternative, exponential, opal dissolution profile (see section 3.4). This exponential dissolution profile for opal has been used in the previous scavenging studies of *Henderson et al.* [1999] and *Marchal et al.* [2000]. Results for the "global" data set using this alternative dissolution profile for opal are illustrated in Figure 7. It is apparent that an equally good fit to this data set can be achieved (σ = 36), but for a very different set of scavenging coefficients. The optimized K values are the following: $K_{CaCO3} = 0$, $K_{opal} = 3.1 \times 10^7$, $K_{POC} = 1.8 \times 10^7$, and $K_{dust} = 0$. Similarly, utilization of the exponential profile in modeling the Pacific Cu data set also predicts significant scavenging by POC. These results support the suggestion that the absence of scavenging by POC in the original model setup relates to the similarity of the POC and opal dissolution profiles. The model is thus insufficiently well constrained to report with certainty on the importance of different particle types to the scavenging of Cu in the ocean. However, we reflect that very good fits to the data can be achieved, indicating an important role for scavenging in the internal cycling of Cu in the ocean. A firmer conclusion to be arrived at with respect to the relative importance of different particle types requires a better knowledge of their dissolution profiles.

6. Discussion and Conclusions

[33] As noted in section 1, this study does not attempt a comprehensive quantitative description of the oceanic biogeochemical cycles of Cu and Zn. In particular, both lateral and vertical transport of dissolved trace metals by water advection are not included, and neither is a major removal process from the upper water column, biological uptake. A further limitation of our approach is that it does not into account the complexation of the transition metals by organic molecules in the dissolved phase. We acknowledge that this assumption may lead to inaccuracies in reported absolute values of scavenging coefficients, but if the size of the ligand-bound pool is relatively invariant with depth, it should affect neither their relative roles nor the modeled profile shapes. To date, there is too little published speciation data available with which to evaluate this assumption on a global scale. Thus, we emphasize that the purpose of this study is not to precisely evaluate scavenging coefficients. Instead, we examine solely whether one end-member vertical process, reversible scavenging, could be responsible for explaining aspects of the *shapes* of the vertical profiles of the two elements.

[34] Despite the simplicity of the approach, the results shown in Figures 2, 3, and 4 show that reversible scavenging can explain the approximately linear vertical distribution of dissolved Cu, at all geographical scales. The model suggests that the key particle types for scavenging of Cu are $CaCO_3$ and opal, with a smaller role for dust. No scavenging is implicated by POC. This observation should be considered provisional, however, due to the similarity of the dissolution profiles of POC and Opal. Indeed, using an alternative dissolution profile parameterization for opal, POC is ascribed a significant role. Sensitivity testing has also highlighted that the relative magnitudes of the scavenging coefficients is contingent on the relative magnitudes of the particle export fluxes, and on the precise selection of the data set to be modeled. Optimized scavenging coefficients reported in this study for Cu thus require independent verification, and should be approached with caution when seeking to apply them directly in future studies.

[35] Mass balance in the reversible scavenging model can be used to estimate the residence time of Cu, via the particle-associated flux (C_p) out of the euphotic zone. Doing so gives an estimated residence time for Cu of circa 20–25,000 years, four or five times longer than the widely cited value calculated from riverine and atmospheric inputs, of 5000 years [*Boyle et al.*, 1977]. The higher the particulate-associated concentration, and larger the export fluxes, the shorter the calculated residence time. Overestimation of the residence time of Cu compared to the published value implies an additional flux of Cu out of the euphotic zone. This additional flux is likely associated with the rapidly sinking, large-particle removal pathway, as described in section 5.2.

[36] In general, the dissolved profiles of Cu are well described by the reversible scavenging model. This is not the case for Zn, however, with the model simulating only relatively linear increases in tracer concentration with depth. Linear shapes are very unlike those observed for Zn, which exhibit low concentrations in surface waters, increasing rapidly toward mid-depth maxima, and high concentrations in deep waters (Figure 2). The Zn profile shape is commonly ascribed to biological uptake in surface waters and regeneration at depth [e.g., *Bruland*, 1980], and this study lends support to the hypothesis that Zn behaves as a true micronutrient [cf. *Yang et al.*, 2012]. The importance of scavenging in controlling dissolved Cu has been recognized previously [*Boyle et al.*, 1977; *Bruland*, 1980; *Craig*, 1974; *Yeats and Campbell*, 1983], with the caveat that biology is likely also playing a role, leading to the labeling of Cu as having "hybrid"-type behavior in seawater [*Bruland and Lohan*, 2003]. Cu is bioessential, and evidence cited for the role of biology in controlling dissolved Cu includes the similarity of cellular and seawater Cu:C ratios [*Sunda and Huntsman*,

1995a]. Taken at face value, however, this study suggests that biological uptake and regeneration is a minor player in the cycling of dissolved Cu.

[37] Another process is clearly of particular significance to Zn in the deep Pacific Ocean, where reversible scavenging cannot explain its high concentrations. This process is lateral water advection. Pacific deep waters are enriched in all of the major nutrients and have the oldest recorded radiocarbon ages in the ocean [*Broecker and Peng*, 1982; *Sarmiento and Gruber*, 2006], explained as the result of their long-term isolation from surface processes. Surface processes deplete nutrients via biological uptake and shuttling to depth (the biological pump), and reset radiocarbon ages via CO_2 exchange with the atmosphere. As deep waters are transported laterally, they act as a reservoir for the nutrients raining down from above, and they "age." The Pacific basin thus has a large inventory of both macronutrients and micronutrients (including Zn), and a long residence time. Cu concentrations are also a factor of 2–3 higher in the deep Pacific compared to the deep Atlantic. It is possible, therefore, that this difference in Cu concentrations is also in part related to the "aging" of Pacific deep waters, despite the success of the scavenging model in replicating dissolved Cu on a global scale. Further work is required to unpick the relative importance of lateral transport and reversible scavenging in controlling the vertical distributions of dissolved Cu in the Pacific.

[38] To summarize, this study supports a dominant role for a reversible scavenging-type process in controlling the vertical cycling of dissolved Cu. Differences in the deep Atlantic and deep Pacific concentrations of Cu may, however, be related in part to the lateral advection of Cu in nutrient-rich deep waters. In contrast to Cu, reversible scavenging is unsuccessful in matching the nutrient-type shape of dissolved Zn profiles, with the model producing only relatively linear increases in tracer concentration with depth. Further, particle scavenging cannot reproduce deep water concentrations of Zn in the Pacific Ocean without arbitrarily increasing the Zn input, highlighting the importance of lateral processes to the global oceanic inventory of Zn.

[39] **Acknowledgments.** The authors would like to thank Gideon Henderson, two anonymous reviewers, and the associate Editor, whose comments and suggestions considerably improved the revised manuscript. This work was supported by NERC studentship NE/H525111/1 to SHL.

References

Anderson, M. A., F. M. M. Morel, and R. R. L. Guillard (1978), Growth limitation of a coastal diatom by low zinc ion activity, *Nature*, *276*(5683), 70–71.

Bacon, M. P., and R. F. Anderson (1982), Distribution of thorium isotopes between dissolved and particulate forms in the deep sea, *J. Geophys. Res., 87*(C3), 2045–2056.

Balistrieri, L., P. G. Brewer, and J. W. Murray (1981), Scavenging residence times of trace metals and surface chemistry of sinking particles in the deep ocean, *Deep Sea Res. Part I*, *28*(2), 101–121.

Berelson, W. M. (2001), Particle settling rates increase with depth in the ocean, *Deep Sea Res. Part II: Topical Studies in Oceanography*, *49*(1), 237–251.

Boyd, P., D. Muggli, D. Varela, R. Goldblatt, R. Chretien, K. Orians, and P. Harrison (1996), In vitro iron enrichment experiments in the NE Subarctic Pacific, *Mar. Ecol. Prog. Ser.*, *136*, 179–193.

Boyle, E. A., F. Sclater, and J. M. Edmond (1976), On the marine geochemistry of cadmium, *Nature*, *263*(5572), 42–44.

Boyle, E. A., F. R. Sclater, and J. M. Edmond (1977), Distribution of dissolved copper in the Pacific, *Earth Planet. Sci. Lett.*, *37*(1), 38–54.

Brand, L. E., W. G. Sunda, and R. R. L. Guillard (1983), Limitation of marine phytoplankton reproductive rates by zinc, manganese, and iron, *Limnol. Oceanogr.*, *28*(6), 1182–1198.

Brand, L. E., W. G. Sunda, and R. R. L. Guillard (1986), Reduction of marine-phytoplankton reproduction rates by copper and cadmium, *J. Exp. Mar. Biol. Ecol.*, *96*(3), 225–250.

Broecker, W., and T.-H. Peng (1982), *Tracers in the Sea*, Eldigo, Lamont-Doherty Geological Observatory, Palisades, NY.

Bruland, K., and Franks (1983), *Trace Elements in Seawater*, chap. 45, pp. 157–215, vol. 8, Academic Press, London.

Bruland, K. W. (1980), Oceanographic distributions of cadmium, zinc, nickel, and copper in the North Pacific, *Earth Planet. Sci. Lett.*, *47*(2), 176–198.

Bruland, K. W. (1989), Complexation of zinc by natural organic ligands in the Central North Pacific, *Limnol. Oceanogr.*, *34*(2), 269–285.

Bruland, K. W., and M. C. Lohan (2003), *Controls of Trace Metals in Seawater*, 23–47, Pergamon, Oxford.

Bruland, K. W., G. A. Knauer, and J. H. Martin (1978), Cadmium in northeast Pacific waters, *Limnol. Oceanogr.*, *23*(4), 618–625.

Bruland, K. W., K. J. Orians, and J. P. Cowen (1994), Reactive trace metals in the stratified central North Pacific, *Geochim. Cosmochim. Acta*, *58*(15), 3171–3182.

Buck, K. N., J. Moffett, K. A. Barbeau, R. M. Bundy, Y. Kondo, and J. Wu (2012), The organic complexation of iron and copper: An intercomparison of competitive ligand exchange–adsorptive cathodic stripping voltammetry (CLE-ACSV) techniques, *Limnol. Oceanogr. Methods*, *10*, 496–515.

Campos, M., and C. M. G. Van den Berg (1994), Determination of copper complexation in sea-water by cathodic stripping voltammetry and ligand competition with salicylaldoxime, *Anal. Chim. Acta*, *284*(3), 481–496.

Catts, J. G., and D. Langmuir (1986), Adsorption of Cu, Pb and Zn by δMnO_2: Applicability of the site binding-surface complexation model, *Appl. Geochem.*, *1*(2), 255–264.

Cave, R. R., C. R. German, J. Thomson, and R. W. Nesbitt (2002), Fluxes to sediments underlying the Rainbow hydrothermal plume at 36°14′N on the Mid-Atlantic Ridge, *Geochim. Cosmochim. Acta*, *66*(11), 1905–1923.

Clegg, S. L., and M. Whitfield (1990), A generalized model for the scavenging of trace metals in the open ocean—I. Particle cycling, *Deep Sea Res. Part A*, *37*(5), 809–832.

Coale, K. H., and K. W. Bruland (1988), Copper complexation in the Northeast Pacific, *Limnol. Oceanogr.*, *33*(5), 1084–1101.

Coale, K. H., and K. W. Bruland (1990), Spatial and temporal variability in copper complexation in the North Pacific, *Deep Sea Res. Part A*, *37*(2), 317–336.

Collier, R., and J. Edmond (1984), The trace element geochemistry of marine biogenic particulate matter, *Prog. Oceanogr.*, *13*(2), 113–199.

Craig, H. (1974), A scavenging model for trace elements in the deep sea, *Earth Planet. Sci. Lett.*, *23*(1), 149–159.

Croot, P. L., O. Baars, and P. Streu (2011), The distribution of dissolved zinc in the Atlantic sector of the Southern Ocean, *Deep Sea Res. Part A*, *58*(25-26), 2707–2719.

Daughney, C. J., S. D. Siciliano, A. N. Rencz, D. Lean, and D. Fortin (2002), Hg(II) adsorption by bacteria: A surface complexation model and its application to shallow acidic lakes and wetlands in Kejimkujik National Park, Nova Scotia, Canada, *Environ. Sci. Technol.*, *36*(7), 1546–1553.

Donat, J. R., and K. W. Bruland (1990), A comparison of two voltammetric techniques for determining zinc speciation in Northeast Pacific Ocean waters, *Mar. Chem.*, *28*(4), 301–323.

Dunne, J. P., R. A. Armstrong, A. Gnanadesikan, and J. L. Sarmiento (2005), Empirical and mechanistic models for the particle export ratio, *Global Biogeochem. Cycles*, *19*, GB4026, doi:10.1029/2004GB002390.

Ellwood, M. J., and K. A. Hunter (2000), The incorporation of zinc and iron into the frustule of the marine diatom Thalassiosira pseudonana, *Limnol. Oceanogr.*, *45*(7), 1517–1524.

Ellwood, M. J., and C. M. G. Van den Berg (2000), Zinc speciation in the Northeastern Atlantic Ocean, *Mar. Chem.*, *68*(4), 295–306.

Ezoe, M., T. Ishita, M. Kinugasa, X. Lai, K. Norisuye, and Y. Sohrin (2004), Distributions of dissolved and acid-dissolvable bioactive trace metals in the North Pacific Ocean, *Geochem. J.*, *38*(6), 535–550.

Fein, J. B., C. J. Daughney, N. Yee, and T. A. Davis (1997), A chemical equilibrium model for metal adsorption onto bacterial surfaces, *Geochim. Cosmochim. Acta*, *61*(16), 3319–3328.

German, C. R., A. C. Campbell, and J. M. Edmond (1991), Hydrothermal scavenging at the Mid-Atlantic Ridge: Modification of trace element dissolved fluxes, *Earth Planet. Sci. Lett.*, *107*(1), 101–114.

German, C. R., S. Colley, M. R. Palmer, A. Khripounoff, and G. P. Klinkhammer (2002), Hydrothermal plume-particle fluxes at 13°N on the East Pacific Rise, *Deep Sea Res. Part A*, *49*(11), 1921–1940.

Ginoux, P., M. Chin, I. Tegen, J. M. Prospero, B. Holben, O. Dubovik, and S.-J. Lin (2001), Sources and distributions of dust aerosols simulated with the GOCART model, *J. Geophys. Res.*, *106*(D17), 20,255–20,273.

Guo, L., P. H. Santschi, M. Baskaran, and A. Zindler (1995), Distribution of dissolved and particulate 230 Th and 232 Th in seawater from the Gulf of Mexico and off Cape Hatteras as measured by SIMS, *Earth Planet. Sci. Lett.*, *133*(1), 117–128.

Henderson, G. M., C. Heinze, R. F. Anderson, and A. M. E. Winguth (1999), Global distribution of the 230 Th flux to ocean sediments constrained by GCM modelling, *Deep Sea Res. Part A*, *46*(11), 1861–1893.

Honeyman, B. D., L. S. Balistrieri, and J. W. Murray (1988), Oceanic trace metal scavenging: The importance of particle concentration, *Deep Sea Res. Part A*, *35*(2), 227–246.

Hunter, K. A. (1983), The adsorptive properties of sinking particles in the deep ocean, *Deep Sea Res. Part A*, *30*(6), 669–675.

Kirkpatrick, S., C. D. Gelatt, and M. P. Vecchi (1983), Optimization by simulated annealing, *Science*, *220*(4598), 671–680.

Krishnaswami, S., D. Lal, B. Somayajulu, R. Weiss, and H. Craig (1976), Large-volume in-situ filtration of deep Pacific waters: Mineralogical and radioisotope studies, *Earth Planet. Sci. Lett.*, *32*(2), 420–429.

Lohan, M. C., P. J. Statham, and D. W. Crawford (2002), Total dissolved zinc in the upper water column of the subarctic North East Pacific, *Deep Sea Res. Part A*, *49*(24-25), 5793–5808.

Löscher, B. M. (1999), Relationships among Ni, Cu, Zn, and major nutrients in the Southern Ocean, *Mar. Chem.*, *67*(1-2), 67–102.

Mangini, A., and R. Key (1983), A 230 Th profile in the Atlantic Ocean, *Earth Planet. Sci. Lett.*, *62*(3), 377–384.

Marchal, O., R. Francois, T. F. Stocker, and F. Joos (2000), Ocean thermohaline circulation and sedimentary 231Pa/230Th ratio, *Paleoceanography*, *15*(6), 625–641.

Martin, J., K. Bruland, and W. Broenkow (1976), *Cadmium Transport in the Califonia Current*, pp. 159–184, Heath, Lexington, Mass.

Martin, J. H., and S. E. Fitzwater (1988), Iron-deficiency limits phytoplankton growth in the northeast Pacific subarctic, *Nature*, *331*(6154), 341–343.

Martin, J. H., G. A. Knauer, D. M. Karl, and W. W. Broenkow (1987), VERTEX: Carbon cycling in the northeast Pacific, *Deep Sea Res. Part A*, *34*(2), 267–285.

Martin, J. H., R. M. Gordon, S. Fitzwater, and W. W. Broenkow (1989), VERTEX: Phytoplankton/iron studies in the Gulf of Alaska, *Deep Sea Res. Part A*, *36*(5), 649–680.

Martin, J. H., S. E. Fitzwater, R. Michael Gordon, C. N. Hunter, and S. J. Tanner (1993), Iron, primary production and carbon-nitrogen flux studies during the JGOFS North Atlantic Bloom Experiment, *Mar. Chem.*, *40*(1-2), 115–134.

Moffett, J. W., and C. Dupont (2007), Cu complexation by organic ligands in the sub-arctic NW Pacific and Bering Sea, *Deep Sea Res. Part I*, *54*(4), 586–595.

Moffett, J. W., R. G. Zika, and L. E. Brand (1990), Distribution and potential sources and sinks of copper chelators in the Sargasso Sea, *Deep Sea Res. Part A*, *37*(1), 27–36.

Moffett, J. W., L. E. Brand, P. L. Croot, and K. A. Barbeau (1997), Cu speciation and cyanobacterial distribution in harbors subject to anthropogenic Cu inputs, *Limnol. Oceanogr.*, *42*(5), 789–799.

Morel, F., A. Milligan, and M. Saito (2003), Marine bioinorganic chemistry: The role of trace metals in the oceanic cycles of major nutrients, in *Treatise on Geochemistry,* vol. 6, edited by H. D. Holland and K. K. Turekian, pp. 113–143, Elsevier, Oxford, U.K.

Morel, F. M. M., and N. M. Price (2003), The biogeochemical cycles of trace metals in the oceans, *Science*, *300*(5621), 944–947.

Morel, F. M. M., R. J. M. Hudson, and N. M. Price (1991), Limitation of productivity by trace-metals in the sea, *Limnol. Oceanogr.*, *36*(8), 1742–1755.

Morel, F. M. M., J. R. Reinfelder, S. B. Roberts, C. P. Chamberlain, J. G. Lee, and D. Yee (1994), Zinc and carbon co-limitation of marine phytoplankton, *Nature*, *369*(6483), 740–742.

Morley, N. H., P. J. Statham, and J. D. Burton (1993), Dissolved trace metals in the southwestern Indian Ocean, *Deep Sea Res. Part A*, *40*(5), 1043–1062.

Nozaki, Y., Y. Horibe, and H. Tsubota (1981), The water column distributions of thorium isotopes in the western North Pacific, *Earth Planet. Sci. Lett.*, *54*(2), 203–216.

Sarmiento, J., and N. Gruber (2006), *Ocean Biogeochemical Dynamics*, 526 pp., Princeton University Press, Princeton, N.J.

Siddall, M., G. M. Henderson, N. R. Edwards, M. Frank, S. A. Möller, T. F. Stocker, and F. Joos (2005), 231Pa/230Th fractionation by ocean transport, biogenic particle flux and particle type, *Earth Planet. Sci. Lett.*, *237*(1-2), 135–155.

Siddall, M., S. Khatiwala, T. van de Flierdt, K. Jones, S. L. Goldstein, S. Hemming, and R. F. Anderson (2008), Towards explaining the Nd paradox using reversible scavenging in an ocean general circulation model, *Earth Planet. Sci. Lett.*, *274*(3-4), 448–461.

Sunda, W. G., and R. R. L. Guillard (1976), Relationship between cupric ion activity and toxicity of copper to phytoplankton, *J. Mar. Res.*, *34*(4), 511–529.

Sunda, W. G., and S. A. Huntsman (1992), Feedback interactions between zinc and phytoplankton in seawater, *Limnol. Oceanogr.*, *37*(1), 25–40.

Sunda, W. G., and S. A. Huntsman (1995a), Regulation of copper concentration in the oceanic nutricline by phytoplankton uptake and regeneration cycles, *Limnol. Oceanogr.*, *40*(1), 132–137.

Sunda, W. G., and S. A. Huntsman (1995b), Iron uptake and growth limitation in oceanic and coastal phytoplankton, *Mar. Chem.*, *50*(1-4), 189–206.

Tessier, A., F. Rapin, and R. Carignan (1985), Trace metals in oxic lake sediments: Possible adsorption onto iron oxyhydroxides, *Geochim. Cosmochim. Acta*, *49*(1), 183–194.

Tessier, A., D. Fortin, N. Belzile, R. R. DeVitre, and G. G. Leppard (1996), Metal sorption to diagenetic iron and manganese oxyhydroxides and associated organic matter: Narrowing the gap between field and laboratory measurements, *Geochim. Cosmochim. Acta*, *60*(3), 387–404.

Trocine, R. P., and J. H. Trefry (1988), Distribution and chemistry of suspended particles from an active hydrothermal vent site on the Mid-Atlantic Ridge at 26°N, *Earth Planet. Sci. Lett.*, *88*(1-2), 1–15.

Tsunogai, S., and M. Minagawa (1978), Settling model for the removal of insoluble chemical elements in seawater, *Geochem. J.*, *12*, 47–56.

Yang, S.-C., D.-C. Lee, and T.-Y. Ho (2012), The isotopic composition of cadmium in the water column of the South China Sea, *Geochim. Cosmochim. Acta*, *98*, 66–77.

Yeats, P. A., and J. A. Campbell (1983), Nickel, copper, cadmium and zinc in the northwest Atlantic Ocean, *Mar. Chem.*, *12*(1), 43–58.

Yeats, P. A., S. Westerlund, and A. R. Flegal (1995), Cadmium, copper and nickel distributions at 4 stations in the eastern central and south Atlantic, *Mar. Chem.*, *49*(4), 283–293.

Zhao, Y. (2011), The carbon cycle and bioactive trace metals in the oceans: Constraints from zinc isotopes, Ph.D. thesis, Earth Sciences, Univ. of Bristol.